

Journal of Visualized Experiments

Quantifying Leukocyte Egress via Lymphatic Vessels from Murine Skin and Tumors --Manuscript Draft--

Article Type:	Invited Methods Article - JoVE Produced Video
Manuscript Number:	JoVE58704R2
Full Title:	Quantifying Leukocyte Egress via Lymphatic Vessels from Murine Skin and Tumors
Keywords:	lymphatic vessels, egress, trafficking, Kaede, FITC paint, leukocytes, melanoma
Corresponding Author:	Amanda W Lund Oregon Health and Science University Portland, OR UNITED STATES
Corresponding Author's Institution:	Oregon Health and Science University
Corresponding Author E-Mail:	lunda@ohsu.edu
Order of Authors:	Maria M. Steele Madeline J Churchill Alec P Breazeale Ryan S Lane Nicholas A Nelson Amanda W Lund
Additional Information:	
Question	Response
Please indicate whether this article will be Standard Access or Open Access.	Standard Access (US\$2,400)
Please indicate the city, state/province, and country where this article will be filmed . Please do not use abbreviations.	Portland, Oregon



August 9, 2018

Dear Dr. Wu,

Please accept our revised manuscript entitled "Quantifying Leukocyte Egress via Lymphatic Vessels from Murine Skin and Tumors" for consideration for publication in *JOVE*.

School of Medicine

Amanda W. Lund, Ph.D.
Assistant Professor; Cell,
Developmental, & Cancer Biology
Knight Cancer Institute
Oregon Center for Spatial Systems
Biomedicine

Mail code L215
3181 SW Sam Jackson Park Road
Portland, OR 97239-3098
tel: 503 494-1095
fax: 503 494-4253

We are thankful to the reviewers for their thoughtful review of our manuscript and include herein a point-by-point response to their comments and a revised manuscript with tracked changes. Notably, we have removed previously published data as per Reviewer #1s request. Additionally, we have addressed all editorial concerns with regards to the protocol, formatting, and have highlighted the relevant parts of the protocol for filming.

Importantly, this work demonstrates the utility of photoconversion for *in vivo* quantitative analysis of broad leukocyte migration from inflamed, infected, and malignant skin. Our comparison to the more broadly applied FITC paint is important to put this assay in context and allow for comparison with previously published literature. Future application of these techniques in the context of inflammation, infection, and tumors will provide important mechanistic insight into the molecular mechanisms that govern leukocyte egress and the functional significance of egress to peripheral tissue inflammation and immunity.

We hope that you find our response to reviewers adequate for publication.

Sincerely,

A handwritten signature in black ink, appearing to read "Amanda W. Lund", is written over a light blue horizontal line.

Amanda W. Lund, PhD.



TITLE:

Quantifying Leukocyte Egress via Lymphatic Vessels from Murine Skin and Tumors

AUTHORS AND AFFILIATIONS:

Maria M. Steele¹, Madeline J. Churchill², Alec P. Breazeale¹, Ryan S. Lane¹, Nicholas A. Nelson¹,
Amanda W. Lund^{1,2,3,4}

¹Department of Cell, Developmental, & Cancer Biology, Oregon Health and Science University,
Portland, OR, USA

²Department of Molecular Microbiology & Immunology, Oregon Health and Science University,
Portland, OR, USA

³Department of Dermatology, Oregon Health and Science University, Portland, OR, USA

⁴Knight Cancer Institute, Oregon Health and Science University, Portland, OR, USA

Corresponding Author:

Amanda W. Lund

Email: lunda@ohsu.edu

Tel: 503-494-1095

Email Addresses of Co-Authors:

Maria M. Steele (steelma@ohsu.edu)

Madeline J. Churchill (madeline@ohsu.edu)

Alec Breazeale (breazeaa@ohsu.edu)

Ryan S. Lane (laner@ohsu.edu)

Nicholas A. Nelson (nanelson@ucsd.edu)

KEYWORDS:

Lymphatic vessels, egress, trafficking, Kaede, FITC paint, leukocytes, melanoma

SUMMARY:

Here, we demonstrate the methods for *in vivo* quantification of leukocyte egress from naïve, inflamed, and malignant murine skin. We perform a head-to-head comparison of two models: transdermal FITC application and *in situ* photoconversion. Furthermore, we demonstrate the utility of photoconversion for tracking leukocyte egress from cutaneous tumors.

ABSTRACT:

Leukocyte egress from peripheral tissues to draining lymph nodes is not only critical for immune surveillance and initiation but also contributes to the resolution of peripheral tissue responses. While a variety of methods are used to quantify leukocyte egress from non-lymphoid, peripheral tissues, the cellular and molecular mechanisms that govern context-dependent egress remain poorly understood. Here, we describe the use of *in situ* photoconversion for quantitative analysis of leukocyte egress from murine skin and tumors. Photoconversion allows for the direct labeling of leukocytes resident within cutaneous tissue. Though skin exposure to violet light induces local inflammatory responses characterized by leukocyte infiltrates and vascular leakiness, in a head-to-head comparison with transdermal

application of fluorescent tracers, photoconversion specifically labeled migratory dendritic cell populations and simultaneously enabled the quantification of myeloid and lymphoid egress from cutaneous microenvironments and tumors. The mechanisms of leukocyte egress remain a missing component in our understanding of intratumoral leukocyte complexity, and thus the application of the tools described herein will provide unique insight into the dynamics of tumor immune microenvironments both at steady state and in response to therapy.

INTRODUCTION:

Peripheral tissue immune responses are shaped not only by leukocyte recruitment to the sites of inflammation but also by mechanisms that regulate their subsequent retention. Thus, protective immunity is dictated by cumulative cellular and molecular mechanisms that determine whether a leukocyte enters, stays within, or rather migrates out of peripheral tissue via lymphatic vessels. Importantly, the propensity for leukocytes to exit tissue through lymphatic vessels (termed egress) is linked to their specialized functions. Dendritic cells (DC) acquire migratory behavior in response to maturation signals leading to antigen transport and presentation in draining lymph nodes (dLN), a process that is necessary for adaptive immunity¹. Scavenging myeloid cells, such as macrophages and neutrophils, serve to clear apoptotic debris through phagocytosis. During bacterial infection, neutrophils egress tissue and ultimately undergo apoptosis in dLNs² and in a model of DSS-induced colitis, data supports the hypothesis that macrophage egress is necessary to resolve local inflammation³. Whether neutrophil and macrophage egress occurs in all inflammatory contexts, however, is unknown. Evidence for T lymphocyte egress from steady state^{4,7}, infected⁸, and inflamed^{4,9-12} peripheral, non-lymphoid tissues indicates that T cells actively recirculate, though the tissue-based signals that drive this exit remain poorly understood. Several studies have identified signals necessary for directional migration towards draining lymphatic capillaries and subsequent egress including chemokine (C-C motif) ligand 21 (CCL21) and its receptor CCR7^{4,11,13}, chemokine (C-X-C motif) ligand 12 (CXCL12) and its receptor CXCR4^{2,14}, and sphingosine-1-phosphate (S1P)^{10,15,16}. These mechanisms are not active in all contexts, however, and whether they determine egress of all cell types remains an open question. Importantly, further insight into the mechanisms that govern egress and its functional relevance in disease requires quantitative *in vivo* methods of analysis.

Several methods have been used to quantify egress in multiple animal models *in vivo* including direct cannulation of lymphatic vessels, adoptive transfer of *ex vivo* labeled leukocytes, transdermal application of fluorescent tracers, injection of labeled particles, and *in vivo* photoconversion^{17,18}. Direct cannulation of afferent mouse lymphatic vessels is difficult and limited in small animals by the volumes of fluid that can be collected. Thus, cannulation has largely been performed in large animals (*e.g.*, sheep) where such surgical manipulations are practical. These studies provide direct evidence for the presence of both lymphoid and myeloid cells in lymph^{10,19,20}. Furthermore, ovine models reveal that acute and chronic inflammation increased lymphocyte presence in lymph by nearly 100-fold^{10,21}.

Adoptive transfer of labeled and genetically manipulated lymphocytes has importantly revealed that CCR7 is required for the egress of CD4⁺ T cells from acutely inflamed skin^{5,11}, while the

pretreatment of lymphocytes with the small molecule S1P receptor agonist, FTY720, only partially inhibits their egress¹⁰. Interestingly, the egress of transferred lymphocytes from chronically inflamed skin is CCR7-independent¹⁰, but may partially require CXCR4⁹. Adoptive transfer experiments, however, deliver non-physiological numbers of *ex vivo* activated and labeled lymphocytes into tissue through injection, which alters the biomechanical environment of tissues and elevated interstitial fluid pressures that open initial lymphatic capillaries and alter their transport properties²². As an alternative, transdermal application of fluorescein isothiocyanate (FITC) in the presence or absence of dermal irritants (*e.g.*, dibutyl phthalate, DBP) or infection^{23,24} allows for the tracking of phagocytic cells that accumulate tracer and migrate to dLNs. Similarly, fluorescently labeled tumors provide a means to track phagocytic cells that have engulfed tumor material²⁵. These methods have provided important insight into the mechanisms that govern DC egress^{13,14,17,26,27} but are unable to track non-phagocytic lymphocytes and, interpretation can be complicated by free lymphatic drainage of soluble FITC thus labeling non-migratory, LN resident DCs.

Alternatively, intravital microscopy is a powerful tool that allows for *in vivo* tracking of physiologically relevant leukocyte populations in real time^{28,29}. Used in combination with the reporter mice and antibody-based *in vivo* immunofluorescent labeling, intravital microscopy has revealed the complex spatial and temporal dynamics of immune cell trafficking, including interstitial migration³⁰, transmigration across the lymphatic endothelium, passage within the lymphatic lumen, and migration upon LN entry^{28,31}. Broad adoption of intravital imaging techniques is limited by expense, necessary expertise for set up, and limited throughput for quantifying multiple cell types. Still, coupling quantitative methods that analyze population dynamics tissues with intravital imaging will provide additional and important mechanistic insight with respect to the mechanisms of motility and migration toward and within lymphatic capillaries^{18,31,32}.

Consequently, *in vivo* photoconversion has emerged as a method that allows for *in situ* labeling, independent of phagocytic activity, and for the quantification of physiological leukocyte egress (when coupled with flow cytometry) in the absence or presence of challenge. Kaede-Tg mice constitutively express a protein isolated from stony coral that exhibits green fluorescence (Kaede green) until exposed to violet light, after which it irreversibly converts to red fluorescence (Kaede red)³³. Photoconverted cells can be tracked as they egress from peripheral tissue sites and accumulate in dLNs. This and other similar photoconvertible mouse models^{34,35} have revealed important biology including constitutive egress of regulatory T cells from skin³⁶, CXCR4-dependent B cell egress from Peyer's patches³⁷, mobilization of resident memory T cells upon peptide re-challenge³⁸, and broad leukocyte egress from tumor microenvironments³⁹. Herein, we perform a head-to-head comparison of photoconversion with transdermal FITC application in the context of cutaneous inflammation and infection to allow for direct comparison of existing data with the photoconvertible method. Furthermore, we demonstrate photoconversion in implanted tumors and describe the conversion efficiency and selective egress from tumor microenvironments. As such, we argue that further application of these methods is needed to elucidate the critical biology of leukocyte egress from tumors, which will have significant implications for interpreting intratumoral leukocyte complexity, anti-tumor

immunity, and response to therapy.

PROTOCOL:

All animal protocols have been approved by the Institutional Animal Care and Use Committee at the Oregon Health & Science University.

1. Induction of Inflammation and FITC Painting of Mouse Pinna

1.1. In a laminar flow hood, anesthetize a C57Bl/6 mouse using vaporized isoflurane (induce at 3-5% isoflurane and maintain at 1-3% isoflurane; oxygen flow rate at 0.5-1.0 L/min). Ensure proper anesthetization by monitoring the loss of pedal reflex, involuntary movements and reduced respiratory rate.

1.2. Lay an ear flat with the ventral side of the ear facing upwards. Pipet 20 μ L of 5% FITC solution dissolved in 1:1 acetone:dibutyl phthalate (DBP) to the ventral side of ear pinna. Allow the ear to dry for a few seconds.

1.3. 24 h after FITC application, euthanize the mice via carbon dioxide exposure followed by cervical dislocation. Collect the ear pinnae into PBS by separating the ears from the head using scissors. Collect the cervical dLNs and inguinal non-draining LNs into PBS using tweezers to separate the LNs from surrounding tissues. Inguinal non-draining LNs will serve as negative controls for the presence of FITC⁺/Kaede red⁺ leukocytes. Dispose of carcasses per institutional protocol.

Note: The optimal time post photoconversion for analysis will depend on the cell type and known migratory behaviors. Dendritic cells, for example, can be detected in dLNs as early as 6 h post DBP application.

2. Induction of Inflammation and Photoconversion of Mouse Pinna

2.1. In a laminar flow hood, anesthetize a Kaede-Tg mouse (background C57Bl/6) by intraperitoneal injection of 80 mg/kg ketamine and 10 mg/kg xylazine dissolved in saline. Ensure proper anesthetization as described in Step 1.1.

2.2. Lay an ear flat with the ventral side of the ear facing upwards. Pipet 20 μ L of a 1:1 acetone:DBP to the ventral side of the ear pinna. Allow the ear to dry for a few seconds.

2.3. After DBP application, cut a slit in a piece of aluminum foil and pull the ear through the slit to expose the ear to the violet light source. Lay the ear flat with the dorsal side facing upward using double-sided tape to secure the ear to the foil.

2.4. Position the ear directly under the light source, and photoconvert for 3 min using a 405 nm light source at 100 mW power.

2.5. 24 h after photoconversion, euthanize the Kaede-Tg mice and harvest the ear pinnae, cervical LNs, and inguinal LNs as described in Step 1.3.

Note: In addition to considerations cited in Step 1.3, the rates of proliferation will determine the timing of analysis as the loss of Kaede red will occur in rapidly dividing cells.

3. Vaccinia Infection of Mouse Pinna and FITC Application

3.1. Anesthetize a C57Bl/6 mouse with vaporized isofluorane as described in Step 1.1.

3.2. Lay the ventral side of the ear flat. Pipet 5×10^6 plaque-forming units (PFU) of vaccinia virus (VacV) diluted in 10 μ L of PBS onto the ear pinna. Using a 29-gauge needle, poke the pinna 25 times⁴⁰.

3.3. 24 h post-infection, anesthetize VacV-infected mice with isofluorane as described in Step 1.1 and pipet 20 μ L 5% FITC dissolved in acetone onto the ventral side of the ear pinna. Allow the ear to dry for a few seconds.

3.4. 24 h after FITC application, euthanize the mice and collect the ear pinnae, cervical LNs and inguinal LNs as described in Step 1.3.

Note: FITC may be applied at any time point post infection to determine DC trafficking at various 24 h intervals. We previously reported that DC migration to dLNs is maintained at similar levels from day 1 to 3 post infection⁴¹.

4. Vaccinia Infection of Mouse Pinna and Photoconversion.

4.1. Anesthetize a Kaede-Tg mouse with vaporized isofluorane as described in Step 1.1.

4.2. Infect the ear pinna with VacV as described in Step 3.2.

4.3. 24 h post-infection, anesthetize VacV-infected Kaede mice as described in Step 2.1 and perform photoconversion as described in Steps 2.3-2.4.

4.4. 24 h after photoconversion, euthanize the mice and harvest the ear pinnae, cervical LNs, and inguinal LNs as described in Step 1.3.

Note: As mentioned above in Step 3.4, photoconversion can be administered at any time point post infection.

5. Ear and Lymph Node Processing for Flow Cytometry

5.1. Create single cell suspensions of ear pinnae: peel apart the ventral and dorsal sides of the ear pinna using two pairs of tweezers and place with the inside of the ear facing down into

the wells of a 24-well plate containing 1 mg/mL collagenase D and 80 U/mL DNase diluted in Hank's Buffered Saline Solution (HBSS) (containing Ca^{2+} and Mg^{2+}). Incubate at 37 °C for 30 min. Press the digested tissue through a 70 μm nylon cell strainer.

5.2. Create single cell suspensions from LNs: place LNs in wells of a 24-well plate containing 1 mg/mL collagenase D and 80 U/mL DNase diluted in HBSS. Tease open the lymph node capsule using two 29-gauge needles, and then incubate the lymph nodes at 37 °C for 30 min. Press the digested tissue through a 70 μm nylon cell strainer.

6. Intradermal Melanoma Tumor Implantation and Photoconversion.

6.1. Shave the fur from the center of the back of a Kaede-Tg mouse using an electric razor.

6.2. Position a 29-gauge needle in the center of the back between the left and right upper scapulae, and intradermally inject 5×10^5 tumor cells (diluted in 50 μL of saline) into the skin of Kaede-Tg mice. Tumors must be carefully positioned to ensure lymphatic drainage to specified lymph nodes (*i.e.*, left and right brachial LNs for tumors placed in the middle of the upper back). Avoid placing the tumor above dLN as this can result in direct photoconversion of the LNs through the skin/tumor.

6.3. Allow the tumors to grow to desired size (100-650 mm^3).

6.4. One day prior to tissue collection, anesthetize a Kaede-Tg mouse as described in 2.1 and shave any newly regrown fur around the tumor.

6.5. Cut a circular hole in aluminum foil and pull the tumor through to expose the tumor to the light source. Cut the hole slightly smaller than the tumor to prevent the tumor from falling back through the hole and minimize the conversion of adjacent, non-tumor skin.

6.6. Position the tumor directly below the light source and photoconvert for 5 min using a 405 nm light source at 200 mW power.

6.7. 24 h after photoconversion, euthanize the mice as described in Step 1.3. Collect the tumors, brachial dLNs, and inguinal non-draining LNs into PBS. Cut the tumors away from the surrounding skin using scissors and remove LNs as described in Step 1.3.

7. Tumor and Lymph Node Processing for Flow Cytometry

7.1. Create single cell suspensions from the tumors: mince the tumors with scissors into wells of a 24-well plate containing 1 mg/mL collagenase D and 80 U/mL DNase diluted in HBSS. Incubate at 37 °C for 1 h. Press the digested tissue through a 70 μm nylon strainer.

7.2. Create single cell suspension of lymph nodes as described in Step 5.2.

8. Antibody Staining for Flow Cytometry

8.1. After digesting the tissues into single cell suspensions, perform standard flow cytometry staining techniques to label the cells with markers of interest. Briefly, pipet 2×10^6 cells into a 96-well plate. Incubate the samples with Fc block (1 $\mu\text{g/mL}$) for 20 min on ice; wash twice with FACs buffer (1% bovine serum albumin in PBS). Add live/dead stain (diluted in PBS) to the samples and incubate for 15 min on ice; wash twice with FACs buffer. Incubate with primary antibodies (**Table of Materials**) diluted in FACs buffer for 30 min on ice; wash twice with FACs buffer.

Note: Kaede green and Kaede red fluorescence overlaps with FITC and PE fluorophores; thus, FITC and PE-conjugated antibodies cannot be used in combination with Kaede proteins.

8.2. After staining, run the samples on a flow cytometer. Alternatively, fix the cells with 2% PFA.

9. Flow Cytometry Analysis

9.1. Set the FITC (Kaede green) and PE (Kaede red) channel PMT voltages to 70-80% of the total range (center population at approximately 10^4) using *ex vivo* Kaede green or Kaede red single-color splenocytes or blood.

Note: Do not compensate for the Kaede green (FITC) and Kaede red (PE) channels as this will result in greater signal spread.

9.1.1. To create single-color Kaede controls, collect a spleen or blood from a Kaede-Tg mouse. Lyse the red blood cells with ACK buffer, then divide the cells into two groups: unconverted Kaede green and converted Kaede red.

9.1.2. For single color Kaede red controls, suspend the cells in 1 mL of PBS and photoconvert in a 24-well plate for 5 min using a 405 nm light sources at a power of 100 mW. Use these cells to set the Kaede green (FITC) and Kaede red PMT voltages on the flow cytometer (Step 9.1).

9.2. Once the voltages for the Kaede proteins has been set, compensate for all other primary antibody stains using single-fluorophore labeled compensation beads per manufacturer's instructions.

9.3. Run the samples on a flow cytometer to collect data.

Note: The Kaede protein is continually being produced by the cells. This means that 24 h after photoconversion, converted cells will be double positive for Kaede green and Kaede red as newly synthesized Kaede (green) protein has accumulated in the cell.

9.4. Analyze the data using FlowJo software or a similar software.

REPRESENTATIVE RESULTS:

We first sought to replicate photoconversion results published in the literature to evaluate the efficiency and determine the associated inflammation in the mouse skin. The ear pinna was exposed to 100 mW violet light (405 nm) for 3 min as previously described³³. Single cell suspensions generated from the ear skin or cervical dLNs immediately following the exposure revealed a 78% conversion efficiency of all CD45⁺ leukocytes in the skin with no converted cells observed in dLNs (**Figure 1A**). To evaluate the inflammatory response associated with photoconversion, we quantified the numbers of infiltrating CD45⁺ leukocytes in converted ears 0 and 24 h post conversion (**Figure 1B**) and acute changes in vascular permeability as measured by Miles's Assay⁴² (**Figure 1C**). Briefly, 200 μ L of 0.5% Evans Blue was intravascularly injected 2 h after photoconversion. The ears were collected 30 min after the injection and Evans Blue was extracted with formamide for 24 h at 55°C (absorbance read at 610 nm⁴²). Both CD45⁺ infiltrates (24 h) and vascular leak (2 h) were significantly increased following the photoconversion, indicating that even at this short exposure, photoconversion itself may impact the tissue-specific inflammatory response. Comparison to CD45⁺ infiltrates (**Figure 1B**) and vascular leak (1.4 μ g/ear \pm 0.75) in VacV infected ears 24 h post infection⁴¹ provides context for the extent of the inflammation caused by violet light (0.08 μ g/ear \pm 0.01).

While several models have been used in various studies to track the leukocyte egress from non-lymphoid, peripheral tissues, it is unclear how these methods compare in their ability to track specific populations as they exit the skin. Consequently, we decided to perform a direct head-to-head comparison of two commonly used methods to track DC egress to LNs, FITC paint and *in vivo* photoconversion, in order to evaluate the efficiency and specificity of each method for quantitative analysis of DC egress at steady state, during cutaneous inflammation, and from infected skin. For each analysis, the skin was subjected to transdermal FITC application or exposed to 100 mW 405 nm light for 3 min. LN DC populations were defined as CD3 ϵ ⁺CD19⁻MHCII⁺CD11c⁺ and further stratified into 1) MHCII^{hi}CD11c^{int} DCs, which enriches for migratory DCs (mDCs) both CD103⁺ BATF3-dependent cross-presenting DCs, and CD11b⁺ dermal DCs; and 2) MHCII^{int}CD11c^{hi} DCs, which enriches for resident DCs (rDCs) including CD8 α ⁺ BATF3-dependent cross-presenting DCs (**Figure 2A**). 24 h after either FITC application or photoconversion, the labeled cells were readily detectable in draining but not non-draining LNs (**Figure 2B**). To quantify the extent of DC migration to LNs and simultaneously determine the specificity of the method for labeling migrating populations and not resident LN populations, we quantified labeled mDCs and rDCs at steady state, 24 h following the application of DBP, and 48 h following VacV scarification (**Figure 2C**). While both photoconversion (Kaede) and FITC labeled mDCs in all conditions, we observed more FITC-labeled than Kaede-labeled mDCs in dLNs, with the exception of VacV infection where the two methods quantified a similar level of egress. Furthermore, in the context of DBP, FITC additionally labeled rDC populations where photoconversion remained specific to mDCs (**Fig. 2C**). Using both of these methods, we observed the egress of approximately 200 DCs from VacV infected skin and importantly noted that this level of egress recapitulates previously published findings using transdermal FITC application by Loo *et al.*⁴¹. Thus, depending on inflammatory context, transdermal FITC application may increase the numbers of labeled DCs detected in dLNs and result in non-

specific labeling of non-migratory LN-resident DC populations, while photoconversion specifically identifies DCs falling into a mDC population.

Kaede-Tg mice have been used to quantify the leukocyte retention in^{5,33,43} and egress from^{5,6,35,38} cutaneous, mucosal, and lymphoid tissues under steady state and inflamed conditions and applied to tumors only in a single publication where the tumors were implanted intradermal into the mouse ears and photoconverted at small volumes³⁹. Thus, we sought to evaluate the utility of *in vivo* photoconversion for the quantification of leukocyte egress from established, large primary tumors to enable further immunological hypothesis testing. First, we implanted MC38 tumor cells intradermally into Kaede-Tg mice between the left and right scapulae. Implantable tumor models enable precise positioning of the tumors to ensure lymphatic drainage to known LNs; tumors placed in the skin of the upper back primarily drain to left and right brachial LNs. After reaching 100 – 150 mm³, the tumors were photoconverted (10 min, 200 mW) and the tumors and dLNs harvested immediately after photoconversion. Analysis by flow cytometry revealed significant conversion of intratumoral CD45⁺ cells from Kaede green⁺ to Kaede red⁺ (69%; **Figure 3A**), while importantly, dLNs remained negative for Kaede red⁺ cells. Immunofluorescence microscopy of photoconverted YUMM 1.7 tumors revealed that photoconversion penetrates deep into the tumor tissue (>1 mm; **Figure 3B**). Interestingly, the skin and vascular cells express high levels of the Kaede protein leading to high photoconversion efficiency of these cell types as seen in **Figure 3B**. This high Kaede red expression makes it difficult to identify the immune cells (both unconverted and converted) using immunofluorescence microscopy.

Given our particular interest in melanoma immunology, we next evaluated the effect of both tumor size and melanin on photoconversion efficiency using various implantable murine tumor cell lines: MC38 (unpigmented colorectal cancer line), B16.F10 (melanin-producing melanoma line), YUMM 1.1 (unpigmented melanoma line), and YUMM 1.7 (unpigmented melanoma line)⁴⁴. Each of these lines were implanted intradermal into Kaede-Tg mice and photoconverted, as described above at various tumor volumes (50 – 650 mm³). The tumors were harvested immediately following the photoconversion and evaluated for the presence of Kaede red CD45⁺ leukocytes by flow cytometry. Interestingly, the photoconversion efficiency of CD45⁺ leukocytes varied significantly across the tumor types and sizes (**Figure 3C**). CD45⁺ leukocytes within small (50 – 150 mm³) YUMM 1.7 and YUMM 1.1 tumors demonstrated the most efficient photoconversion at 80% and 60%, respectively. As the volumes increased for these tumors, the conversion efficiencies decreased to around 50% for large tumors (> 600 mm³). Melanin had a striking impact on photoconversion efficiency: maximum photoconversion for CD45⁺ cells within melanin-producing B16.F10 tumors was only about 30% and dropped to 10% as the tumors reached volumes of 400 mm³. Interestingly, analysis of intratumoral CD8⁺ T cells revealed photoconversion efficiency for these cells at nearly 80 – 90% in small tumors regardless of melanin production (**Figure 3D**). For unpigmented tumors, CD8⁺ T cell conversion remained high even as the tumors reached large volumes, but decreased significantly with the size when the melanin was present. As such, the utility of B16.F10 murine melanomas, and other melanin-producing melanoma lines, may be limited to small tumors (50 mm³), which is consistent with the biological function of melanin in absorbing light. To evaluate the

inflammatory response associated with the photoconversion of tumors, we quantified the number of CD45⁺ cells in unconverted tumors and converted tumors 24 h post photoconversion (**Figure 3E**). We saw no significant difference in the total numbers of CD45⁺ cells detected in the tumors 24 h following the photoconversion compared to unconverted tumors.

We next quantified the leukocyte egress from tumor microenvironments using Kaede-Tg mice, which allows for the interrogation of trafficking behavior of both myeloid and lymphoid cell types. MC38 or YUMM 1.7 tumor cells were intradermally implanted into Kaede-Tg mice. The tumors were photoconverted once the volumes reached between 100 – 150 mm³ (5 min, 200 mW); brachial dLNs and inguinal non-draining LNs were collected 24 h after the photoconversion. Intratumoral leukocyte populations were quantified from MC38 and YUMM 1.7 tumors implanted into control C57Bl/6 mice and collected once the tumors reached 100 – 150 mm³. We evaluated the leukocyte complexity within the tumors and egressed populations by flow cytometry: T cells (CD3 ϵ ⁺CD4⁺/CD8⁺), B cells (CD3 ϵ ⁺CD19⁺), DCs (CD11c⁺MHCII⁺CD11b⁺), neutrophils (CD11b⁺MHCII⁺Ly6G⁺), macrophages (CD11b⁺MHCII⁺F4/80⁺), and inflammatory monocytes (CD11b⁺Ly6G⁺Ly6C⁺; **Figure 4A**). Using this same gating scheme, we evaluated the percent of each leukocyte population in dLNs that expressed Kaede red indicating previous residence in tumor microenvironments (**Figure 4B**). Interestingly, while both MC38 (**Figure 4C**) and YUMM 1.7 (**Figure 4D**) tumors were mainly infiltrated with the myeloid cells (monocytes, DCs, and macrophages), approximately 50% of the cells that had egressed from both tumor types were T lymphocytes (both CD4⁺ and CD8⁺). In addition to T cells, we also observed DCs, B cells, and monocytes within egressed populations from the tumors but macrophages and neutrophils were not detected from either tumor type. Altogether, this data demonstrates the utility of Kaede-Tg photoconvertible mice for tracking multiple leukocyte lineages in an endogenous setting. Furthermore, our analysis indicates that egress is a selective, active process that may have significant implications for determining intratumoral leukocyte complexity.

FIGURE AND TABLE LEGENDS:

Figure 1: Photoconversion efficiency and associated inflammation in murine skin. Murine dermis was photoconverted for 3 min at 100 mW (405 nm light). **(A)**. Representative flow plots depicting photoconverted (Kaede red⁺) CD45⁺ cells from an unconverted and converted ear and cervical dLN immediately following photoconversion. Populations were pre-gated on live, CD45⁺ single cells. **(B)**. Enumeration of total CD45⁺ cells in unconverted ears, ears collected immediately following photoconversion, ears collected 24 h after photoconversion, and ears collected 24 h after VacV infection (n = 3). **(C)**. A Miles's assay was performed to quantify vascular leakiness immediately following the exposure to 405 nm light (3 min, 100 mW). Representative image of leakage in ear skin (left) and quantification of extracted dye (right) (n=3). Error bars represent SEM. *p<0.05 and **p<0.01.

Figure 2: DC egress from naïve, inflamed, and infected skin. **(A)**. Gating scheme to identify migratory DCs (mDCs; MHCII^{hi}CD11c^{int}) and resident DCs (rDCs; MHCII^{hi}CD11c^{hi}). **(B)**. Representative flow plots indicating FITC⁺ or Kaede red⁺ DCs, pre-gated on mDCs, from the mice infected with VacV (dLN) or contralateral non-draining LN controls. **(C)**. Quantification of the

numbers of Kaede red⁺ and FITC⁺ mDCs and rDCs in dLNs of steady state, DBP-inflamed (24 h post application), and VacV infected skin (48 h post infection). Error bars represent SEM.

Figure 3: Photoconversion efficiency in tumor microenvironments. Tumors were photoconverted for 10 min at 200 mW (405 nm light). **(A).** Representative flow plots of Kaede green and Kaede red in unconverted and converted MC38 tumors and brachial dLN immediately following photoconversion. Populations were pre-gated on live, CD45⁺ single-cells. **(B).** Immunofluorescence microcopy of frozen, OCT-embedded YUMM 1.7 tumors both unconverted and photoconverted. Scale bar = 200 μ m. **(C)** Conversion efficiency of CD45⁺ leukocytes and **(D)** CD8⁺ lymphocytes in melanin-producing (B16.F10) and unpigmented (MC38, YUMM 1.1, YUMM 1.7). Each point represents a single mouse. **(E).** Enumeration of total CD45⁺ cells in unconverted tumors and photoconverted tumors collected 24 h after photoconversion (n = 3). Error bars represent SEM.

Figure 4: Leukocyte egress from tumor microenvironments is selective. **(A).** Gating scheme for identifying myeloid and lymphoid populations in MC38 dLNs. **(B).** Representative flow plots identifying Kaede red⁺ cells among myeloid and lymphoid cells in MC38 dLNs 24 h after photoconversion. Percentages in flow plots indicate the frequency of Kaede red⁺ cells within the indicated parent leukocyte population in LNs. **(C, D).** Relative proportions of intratumoral (% of CD45⁺ cells) and egressed (% Kaede red⁺ cells; brachial dLNs) leukocytes from MC38 **(C, n = 3)** and YUMM 1.7 **(D, n = 4)** tumors.

DISCUSSION:

Although the leukocyte egress from peripheral, non-lymphoid tissues is critical for the initiation and resolution of immune responses, the molecular mechanisms that govern egress are poorly understood. This gap in knowledge is largely due to ready availability of tools for the quantification *in vivo*. Here, we describe the use of photoconvertible mice (Kaede-Tg) to quantify endogenous leukocyte egress from the skin and tumors and provide a direct head-to-head comparison with FITC paint in inflammatory and infection models. We demonstrate that while both models track endogenous DC populations, free drainage of FITC and poor uptake by non-phagocytic cells limits the utility of FITC paint for broad analysis of myeloid and lymphoid egress from peripheral, non-lymphoid tissues including tumors. Moreover, we present the data that indicates the egress from the tumors is selective rather than stochastic thus confirming findings presented by Torcellan *et al.*³⁹. Further investigation of the mechanisms governing leukocyte egress from tumors may reveal novel insight into tumor-associated inflammation and immunity.

We first evaluated the efficiency of photoconversion in murine skin and its effect on local inflammation when using settings reported in literature. The exposure of ears to violet light for 3 min at 100 mW power resulted in efficient photoconversion of CD45⁺ cells within the ear skin (78%) with no conversion in downstream dLNs. Reports in the literature demonstrate the 3-5 min exposure is optimal for cutaneous tissues^{5,33,38}. However, this exposure led to increased numbers of CD45⁺ cells in the ear pinna 24 h following the conversion and vascular leakage indicating that photoconversion at these settings in ear skin induces local inflammation, which

should be considered when interpreting data. We next sought to directly compare DC trafficking to LNs using both Kaede photoconversion and the more broadly utilized FITC paint assay^{23,24} at steady-state, during DBP-induced inflammation, and from VacV infected ears. We observed elevated labeling in FITC treated as compared to photoconverted skin at steady state and following DBP treatment. Application of free FITC to skin can result in direct drainage via lymphatic vessels to draining LNs where resident DC populations, that do not migrate (*e.g.*, CD8 α ⁺ DCs), sample FITC. Consistent with this, we observed significant numbers of rDCs with FITC label when treated with the irritant DBP. In contrast, Kaede red-labeled DCs were only observed in the mDC population following the photoconversion indicating that photoconversion provides a more specific way to label mDCs. Even within the mDC population, however, we observed quantitatively more labeled mDCs when using FITC over photoconversion. While this may also be explained by free FITC drainage, it is possible that the differences in the period of labeling, where the photoconversion can only label DCs currently resident in skin while FITC remains in the skin for the duration of the 24 h period, accounts for the differences in observed mDC egress. Interestingly, in the context of viral infection, both photoconversion and FITC application measured relatively equal levels of mDC egress and few FITC⁺ rDCs in the LNs draining VacV-infected ears. We recently reported that lymphatic drainage is significantly reduced following VacV infection, and thus the viral-induced reduction in lymphatic transport may improve the specificity of FITC paint and reduced labeling of LN resident DC populations³¹. Importantly, this work also highlights the fact that within the mDC population (CD3 ϵ ⁻CD19⁻MHCII^{hi}CD11c^{int}), the number of DCs that have actively migrated within 24 h is a minor population and thus total mDC numbers are not a good surrogate for active migration⁴¹. Finally, it is interesting to note that we consistently quantify mDC egress at around 200 cells for any given 24 h period following VacV infection⁴¹, while 1500-2000 DCs egress from tumor microenvironments. Given the tremendous efficacy of VacV as a vaccine platform, particularly when applied by scarification⁴⁵⁻⁴⁷, it is interesting to speculate that it is the quality of the DC and perhaps the type of DC presenting antigen, rather than the quantity, that determines robust protective immunity.

Leukocyte egress from tumor microenvironments, beyond DCs^{25,48}, remains a poorly investigated area. Although the tumors are considered chronically inflamed microenvironments, whether similar mechanisms regulate cellular egress from non-malignant and malignant tissues remains unknown. Furthermore, whether leukocyte egress from tumors is stochastic or rather selective will have significant implications for interpreting leukocyte accumulation and retention in tumor microenvironments. As such, leukocyte egress from tumors may be crucial to understanding how tumors evade immune surveillance and lead to novel strategies for immunotherapy. Here we apply the photoconvertible Kaede-Tg model to study leukocyte egress from implantable cutaneous tumors, where FITC paint would be insufficient to broadly label both myeloid and lymphoid populations. Initial studies revealed that photoconversion efficiency in implanted tumors was dependent both upon tumor size and melanin. While photoconversion efficiency rapidly drops off as tumors grow when melanin is present (B16.F10), non-pigmented tumor lines such as the YUMM and MC38 tumors exhibit more stable conversion efficiency across tumor sizes tested. Interestingly, we observed improved conversion efficiency in the CD8⁺ T cell compartment compared to CD45⁺ cells, which

declined as tumors increased in size. There are likely several factors contributing to this observation. First, the location within a tumor will impact the exposure and thus the conversion efficiency of particular cell types. T cells are frequently found restricted to the skin-tumor interface in implantable tumor models and thus may be more readily photoconverted relative to myeloid cells infiltrating the tumor parenchyma. Secondly, not all leukocytes express the same levels of the Kaede protein⁴⁹ and thus may not all be equally detected by flow cytometry; this may lead to lower observed percentages of photoconversion when analyzing a more heterogeneous cell population such as all CD45⁺ cells. Finally, it is important to note that data presented in **Figure 3** was generated following 10 min of violet light exposure. This initial exposure time was chosen based on reports in the literature citing photoconversion times for various organs including skin, LNs, mucosal tissues, and tumors^{5,6,33,35,39,43}. The only other study employing the photoconvertible system in tumors, photoconversion was performed for 20 min³⁹. Further optimization in our hands revealed improved efficiency with a shortened exposure time of 5 min for both small and large volumes. It is likely that prolonged exposure leads to photobleaching of Kaede fluorescence, and as such, our reported conversion efficiencies may be underestimates. Prolonged exposure may also lead to increased photoconversion-associated inflammation and confound study results. Tumors photoconverted for 5 min demonstrated no significant difference in the number of intratumoral CD45⁺ cells 24 h after photoconversion compared to unconverted tumors. Additionally, the tumors photoconverted for 5 min demonstrated measurable and reproducible egress for both myeloid and lymphoid populations. Consequently, individual optimization within specific tissues or tumors of interest is necessary to achieve optimal results.

Lastly, we used *in situ* photoconversion to quantify endogenous leukocyte egress from tumors implanted into Kaede-Tg mice. Using two different implantable, non-pigmented tumor models we observed significant egress of DCs, T cells, and monocytes. Consistent with recently published work³⁹, both CD4⁺ and CD8⁺ T cells egressed from tumor microenvironments along with a significant number of double negative CD3ε⁺ T cells. At least, one component of this population may be gamma delta T cells as previously described³⁹, though the functional significance of this observation remains to be determined. Importantly, when we compared the proportions of leukocytes egressing from tumors to the relative proportions of leukocytes present within the tumor microenvironments, we observed leukocyte enrichment in egressed populations relative to intratumoral pools in both models indicating selective leukocyte egress. Notably, macrophages and neutrophils were absent in egressed populations, though both cell types have been described to egress under inflamed and infected conditions^{2,50-54} and are significant contributors to intratumoral leukocyte repertoires^{39,55,56}. Thus, the leukocyte egress from the tumors can be quantified using photoconvertible models, is not stochastic but rather a regulated process, and remains an important and understudied biology with significant implications for understanding inflammatory and immune dynamics in tumor microenvironments at steady state and in response to therapy.

ACKNOWLEDGMENTS:

The authors would like to thank Dr. Marcus Bosenberg for providing YUMM 1.1 and YUMM 1.7 murine melanoma lines and Dr. Deborah J. Fowell for providing B6.Cg-Tg(CAG-tdKaede)15Utr

mice in agreement with RIKEN BRC through the National Bio-Resource of the MEXT, Japan.

DISCLOSURES:

The authors have no conflicts to disclose.

REFERENCES:

- 1 Banchereau, J. & Steinman, R. M. Dendritic cells and the control of immunity. *Nature*. **392** (6673), 245-252, (1998).
- 2 Hampton, H. R., Bailey, J., Tomura, M., Brink, R. & Chtanova, T. Microbe-dependent lymphatic migration of neutrophils modulates lymphocyte proliferation in lymph nodes. *Nature Communications*. **6** 7139, (2015).
- 3 D'Alessio, S. *et al.* VEGF-C-dependent stimulation of lymphatic function ameliorates experimental inflammatory bowel disease. *Journal of Clinical Investigation*. **124** (9), 3863-3878, (2014).
- 4 Debes, G. F. *et al.* Chemokine receptor CCR7 required for T lymphocyte exit from peripheral tissues. *Nature Immunology*. **6** (9), 889-894, (2005).
- 5 Bromley, S. K., Yan, S., Tomura, M., Kanagawa, O. & Luster, A. D. Recirculating memory T cells are a unique subset of CD4+ T cells with a distinct phenotype and migratory pattern. *Journal of Immunology*. **190** (3), 970-976, (2013).
- 6 Tomura, M. *et al.* Activated regulatory T cells are the major T cell type emigrating from the skin during a cutaneous immune response in mice. *Journal of Clinical Investigation*. **120** (3), 883-893, (2010).
- 7 Tomura, M., Itoh, K. & Kanagawa, O. Naive CD4+ T lymphocytes circulate through lymphoid organs to interact with endogenous antigens and upregulate their function. *Journal of Immunology*. **184** (9), 4646-4653, (2010).
- 8 Jennrich, S., Lee, M. H., Lynn, R. C., Dewberry, K. & Debes, G. F. Tissue exit: a novel control point in the accumulation of antigen-specific CD8 T cells in the influenza A virus-infected lung. *Journal of Virology*. **86** (7), 3436-3445, (2012).
- 9 Geherin, S. A., Wilson, R. P., Jennrich, S. & Debes, G. F. CXCR4 is dispensable for T cell egress from chronically inflamed skin via the afferent lymph. *PLoS One*. **9** (4), e95626, (2014).
- 10 Brown, M. N. *et al.* Chemoattractant receptors and lymphocyte egress from extralymphoid tissue: changing requirements during the course of inflammation. *Journal of Immunology*. **185** (8), 4873-4882, (2010).
- 11 Bromley, S. K., Thomas, S. Y. & Luster, A. D. Chemokine receptor CCR7 guides T cell exit from peripheral tissues and entry into afferent lymphatics. *Nature Immunology*. **6** (9), 895-901, (2005).
- 12 Gomez, D., Diehl, M. C., Crosby, E. J., Weinkopff, T. & Debes, G. F. Effector T Cell Egress via Afferent Lymph Modulates Local Tissue Inflammation. *Journal of Immunology*. **195** (8), 3531-3536, (2015).
- 13 Ohl, L. *et al.* CCR7 governs skin dendritic cell migration under inflammatory and steady-state conditions. *Immunity*. **21** (2), 279-288, (2004).
- 14 Kabashima, K. *et al.* CXCL12-CXCR4 engagement is required for migration of cutaneous dendritic cells. *American Journal of Pathology*. **171** (4), 1249-1257, (2007).

617 15 Cyster, J. G. & Schwab, S. R. Sphingosine-1-phosphate and lymphocyte egress from
618 lymphoid organs. *Annual Review of Immunology*. **30** 69-94, (2012).

619 16 Matloubian, M. *et al.* Lymphocyte egress from thymus and peripheral lymphoid organs
620 is dependent on S1P receptor 1. *Nature*. **427** (6972), 355-360, (2004).

621 17 Teijeira, A., Rouzaut, A. & Melero, I. Initial afferent lymphatic vessels controlling
622 outbound leukocyte traffic from skin to lymph nodes. *Frontiers in Immunology*. **4** 433,
623 (2013).

624 18 Hunter, M. C., Teijeira, A. & Halin, C. T Cell Trafficking through Lymphatic Vessels.
625 *Frontiers in Immunology*. **7** 613, (2016).

626 19 Bujdoso, R., Hopkins, J., Dutia, B. M., Young, P. & McConnell, I. Characterization of sheep
627 afferent lymph dendritic cells and their role in antigen carriage. *Journal of Experimental*
628 *Medicine*. **170** (4), 1285-1301, (1989).

629 20 Young, A. J. The physiology of lymphocyte migration through the single lymph node in
630 vivo. *Seminars in Immunology*. **11** (2), 73-83, (1999).

631 21 Seabrook, T. *et al.* The traffic of resting lymphocytes through delayed hypersensitivity
632 and chronic inflammatory lesions: a dynamic equilibrium. *Seminars in Immunology*. **11**
633 (2), 115-123, (1999).

634 22 Swartz, M. A. *et al.* Mechanics of interstitial-lymphatic fluid transport: theoretical
635 foundation and experimental validation. *Journal of Biomechanics*. **32** (12), 1297-1307,
636 (1999).

637 23 Macatonia, S. E., Knight, S. C., Edwards, A. J., Griffiths, S. & Fryer, P. Localization of
638 antigen on lymph node dendritic cells after exposure to the contact sensitizer
639 fluorescein isothiocyanate. Functional and morphological studies. *Journal of*
640 *Experimental Medicine*. **166** (6), 1654-1667, (1987).

641 24 Robbiani, D. F. *et al.* The leukotriene C(4) transporter MRP1 regulates CCL19 (MIP-3beta,
642 ELC)-dependent mobilization of dendritic cells to lymph nodes. *Cell*. **103** (5), 757-768,
643 (2000).

644 25 Roberts, E. W. *et al.* Critical Role for CD103(+)/CD141(+) Dendritic Cells Bearing CCR7 for
645 Tumor Antigen Trafficking and Priming of T Cell Immunity in Melanoma. *Cancer Cell*. **30**
646 (2), 324-336, (2016).

647 26 Forster, R. *et al.* CCR7 coordinates the primary immune response by establishing
648 functional microenvironments in secondary lymphoid organs. *Cell*. **99** (1), 23-33, (1999).

649 27 Johnson, L. A. & Jackson, D. G. The chemokine CX3CL1 promotes trafficking of dendritic
650 cells through inflamed lymphatics. *Journal of Cell Science*. **126** (Pt 22), 5259-5270,
651 (2013).

652 28 Teijeira, A. *et al.* T Cell Migration from Inflamed Skin to Draining Lymph Nodes Requires
653 Intralymphatic Crawling Supported by ICAM-1/LFA-1 Interactions. *Cell Reports*. **18** (4),
654 857-865, (2017).

655 29 Kilarski, W. W. *et al.* Intravital immunofluorescence for visualizing the microcirculatory
656 and immune microenvironments in the mouse ear dermis. *PLoS One*. **8** (2), e57135,
657 (2013).

658 30 Overstreet, M. G. *et al.* Inflammation-induced interstitial migration of effector CD4(+) T
659 cells is dependent on integrin alphaV. *Nature Immunology*. **14** (9), 949-958, (2013).

660 31 Russo, E. *et al.* Intralymphatic CCL21 Promotes Tissue Egress of Dendritic Cells through
661 Afferent Lymphatic Vessels. *Cell Reports*. **14** (7), 1723-1734, (2016).

662 32 Steven, P., Bock, F., Huttmann, G. & Cursiefen, C. Intravital two-photon microscopy of
663 immune cell dynamics in corneal lymphatic vessels. *PLoS One*. **6** (10), e26253, (2011).

664 33 Tomura, M. *et al.* Monitoring cellular movement in vivo with photoconvertible
665 fluorescence protein "Kaede" transgenic mice. *Proceedings of the National Academy of
666 Sciences of the USA*. **105** (31), 10871-10876, (2008).

667 34 Shand, F. H. *et al.* Tracking of intertissue migration reveals the origins of tumor-
668 infiltrating monocytes. *Proceedings of the National Academy of Sciences of the USA*. **111**
669 (21), 7771-7776, (2014).

670 35 Tomura, M. *et al.* Tracking and quantification of dendritic cell migration and antigen
671 trafficking between the skin and lymph nodes. *Scientific Reports*. **4** 6030, (2014).

672 36 Moran, A. E. *et al.* T cell receptor signal strength in Treg and iNKT cell development
673 demonstrated by a novel fluorescent reporter mouse. *Journal of Experimental Medicine*.
674 **208** (6), 1279-1289, (2011).

675 37 Schmidt, T. H., Bannard, O., Gray, E. E. & Cyster, J. G. CXCR4 promotes B cell egress from
676 Peyer's patches. *Journal of Experimental Medicine*. **210** (6), 1099-1107, (2013).

677 38 Beura, L. K. *et al.* T Cells in Nonlymphoid Tissues Give Rise to Lymph-Node-Resident
678 Memory T Cells. *Immunity*. **48** (2), 327-338 e325, (2018).

679 39 Torcellan, T. *et al.* In vivo photolabeling of tumor-infiltrating cells reveals highly
680 regulated egress of T-cell subsets from tumors. *Proceedings of the National Academy of
681 Sciences of the USA*. **114** (22), 5677-5682, (2017).

682 40 Khan, T. N., Mooster, J. L., Kilgore, A. M., Osborn, J. F. & Nolz, J. C. Local antigen in
683 nonlymphoid tissue promotes resident memory CD8+ T cell formation during viral
684 infection. *Journal of Experimental Medicine*. **213** (6), 951-966, (2016).

685 41 Loo, C. P. *et al.* Lymphatic Vessels Balance Viral Dissemination and Immune Activation
686 following Cutaneous Viral Infection. *Cell Reports*. **20** (13), 3176-3187, (2017).

687 42 Radu, M. & Chernoff, J. An in vivo assay to test blood vessel permeability. *Journal of
688 Visualized Experiments*. 10.3791/50062 (73), e50062, (2013).

689 43 Morton, A. M. *et al.* Endoscopic photoconversion reveals unexpectedly broad leukocyte
690 trafficking to and from the gut. *Proceedings of the National Academy of Sciences of the
691 USA*. **111** (18), 6696-6701, (2014).

692 44 Meeth, K., Wang, J. X., Micevic, G., Damsky, W. & Bosenberg, M. W. The YUMM lines: a
693 series of congenic mouse melanoma cell lines with defined genetic alterations. *Pigment
694 Cell Melanoma Research*. **29** (5), 590-597, (2016).

695 45 Demkowicz, W. E., Jr., Littaua, R. A., Wang, J. & Ennis, F. A. Human cytotoxic T-cell
696 memory: long-lived responses to vaccinia virus. *Journal of Virology*. **70** (4), 2627-2631,
697 (1996).

698 46 Stewart, A. J. & Devlin, P. M. The history of the smallpox vaccine. *Journal of Infection*. **52**
699 (5), 329-334, (2006).

700 47 Hammarlund, E. *et al.* Duration of antiviral immunity after smallpox vaccination. *Nature
701 Medicine*. **9** (9), 1131-1137, (2003).

702 48 Lund, A. W. *et al.* Lymphatic vessels regulate immune microenvironments in human and
703 murine melanoma. *Journal of Clinical Investigation*. **126** (9), 3389-3402, (2016).

704 49 Tomura, M. & Kabashima, K. Analysis of cell movement between skin and other
705 anatomical sites in vivo using photoconvertible fluorescent protein "Kaede"-transgenic
706 mice. *Methods in Molecular Biology*. **961** 279-286, (2013).

707 50 Bellingan, G. J., Caldwell, H., Howie, S. E., Dransfield, I. & Haslett, C. In vivo fate of the
708 inflammatory macrophage during the resolution of inflammation: inflammatory
709 macrophages do not die locally, but emigrate to the draining lymph nodes. *Journal of*
710 *Immunology*. **157** (6), 2577-2585, (1996).

711 51 Gautier, E. L., Ivanov, S., Lesnik, P. & Randolph, G. J. Local apoptosis mediates clearance
712 of macrophages from resolving inflammation in mice. *Blood*. **122** (15), 2714-2722,
713 (2013).

714 52 Abadie, V. *et al.* Neutrophils rapidly migrate via lymphatics after Mycobacterium bovis
715 BCG intradermal vaccination and shuttle live bacilli to the draining lymph nodes. *Blood*.
716 **106** (5), 1843-1850, (2005).

717 53 Beauvillain, C. *et al.* CCR7 is involved in the migration of neutrophils to lymph nodes.
718 *Blood*. **117** (4), 1196-1204, (2011).

719 54 Rigby, D. A., Ferguson, D. J., Johnson, L. A. & Jackson, D. G. Neutrophils rapidly transit
720 inflamed lymphatic vessel endothelium via integrin-dependent proteolysis and lipoxin-
721 induced junctional retraction. *Journal of Leukocyte Biology*. **98** (6), 897-912, (2015).

722 55 Hanahan, D. & Coussens, L. M. Accessories to the crime: functions of cells recruited to
723 the tumor microenvironment. *Cancer Cell*. **21** (3), 309-322, (2012).

724 56 Binnewies, M. *et al.* Understanding the tumor immune microenvironment (TIME) for
725 effective therapy. *Nature Medicine*. **24** (5), 541-550, (2018).

726

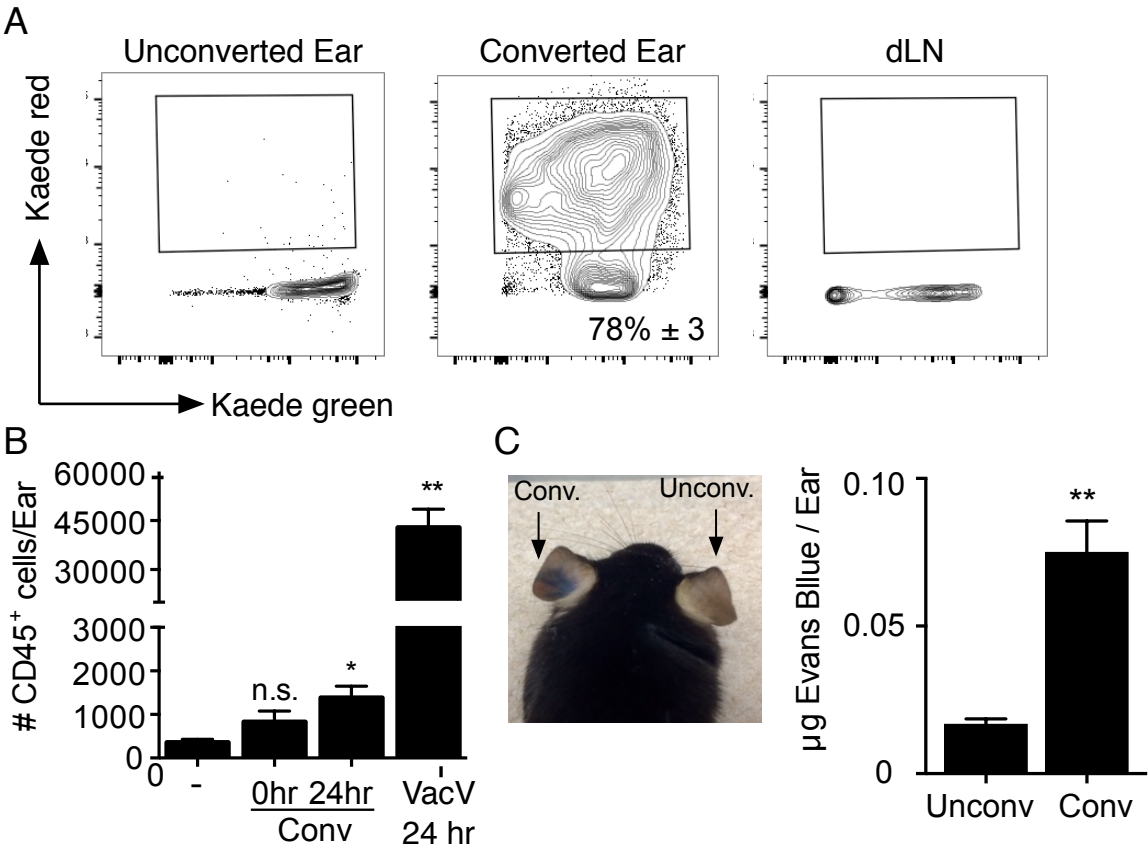


Figure 2

[Click here to access/download;Figure;Figure 2.pdf](#)

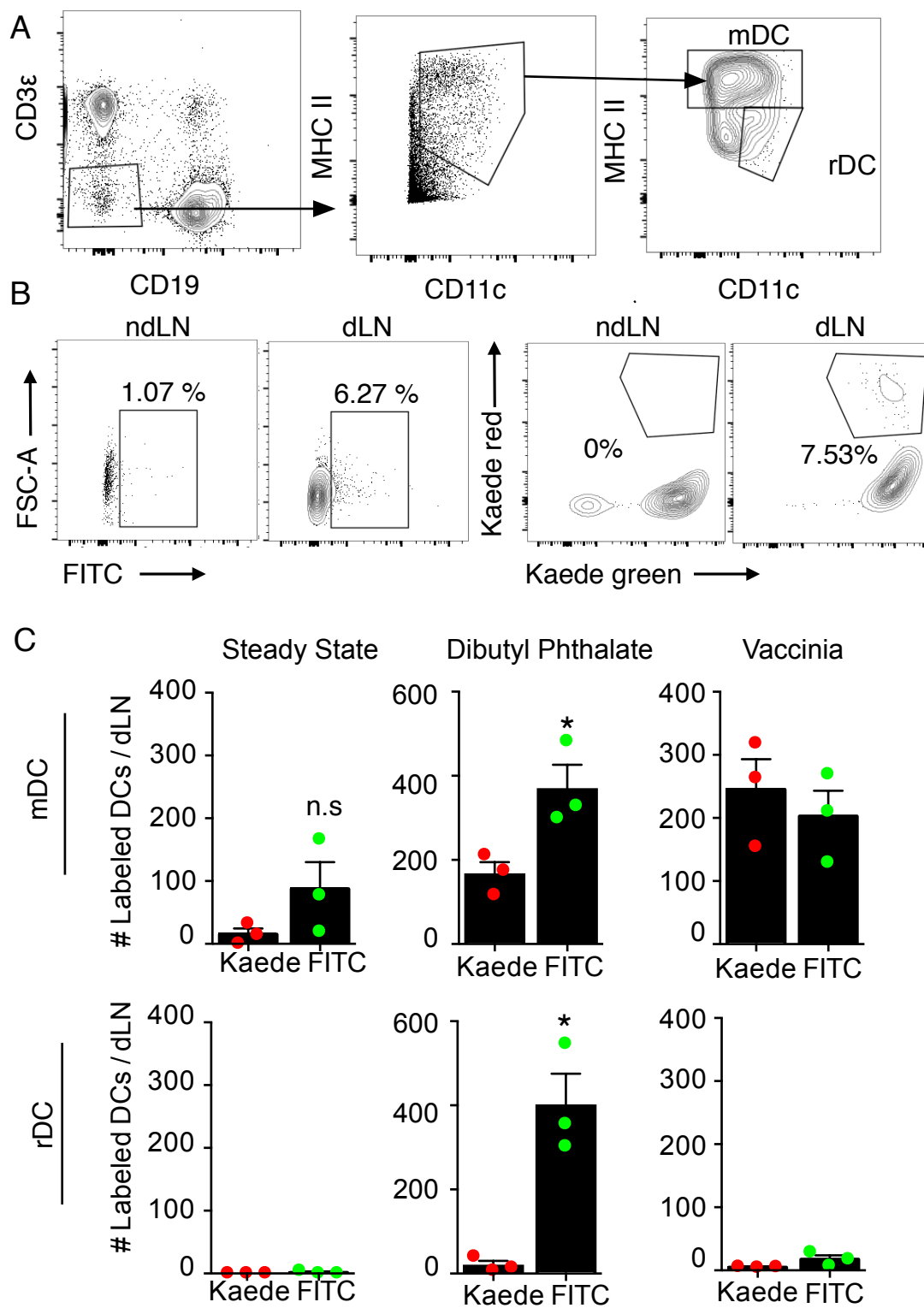


Figure 3

[Click here to access/download;Figure;Figure 3.pdf](#)

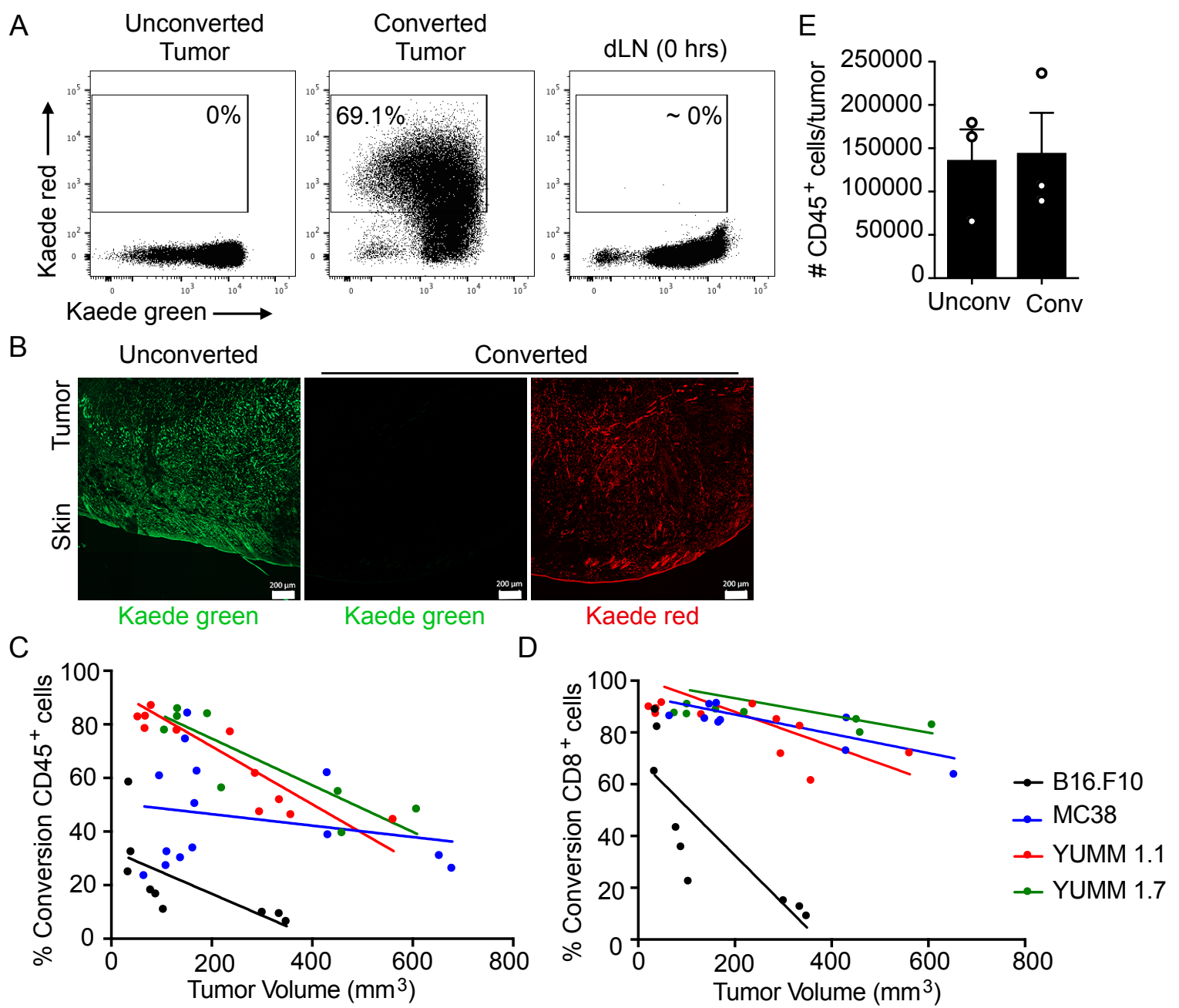
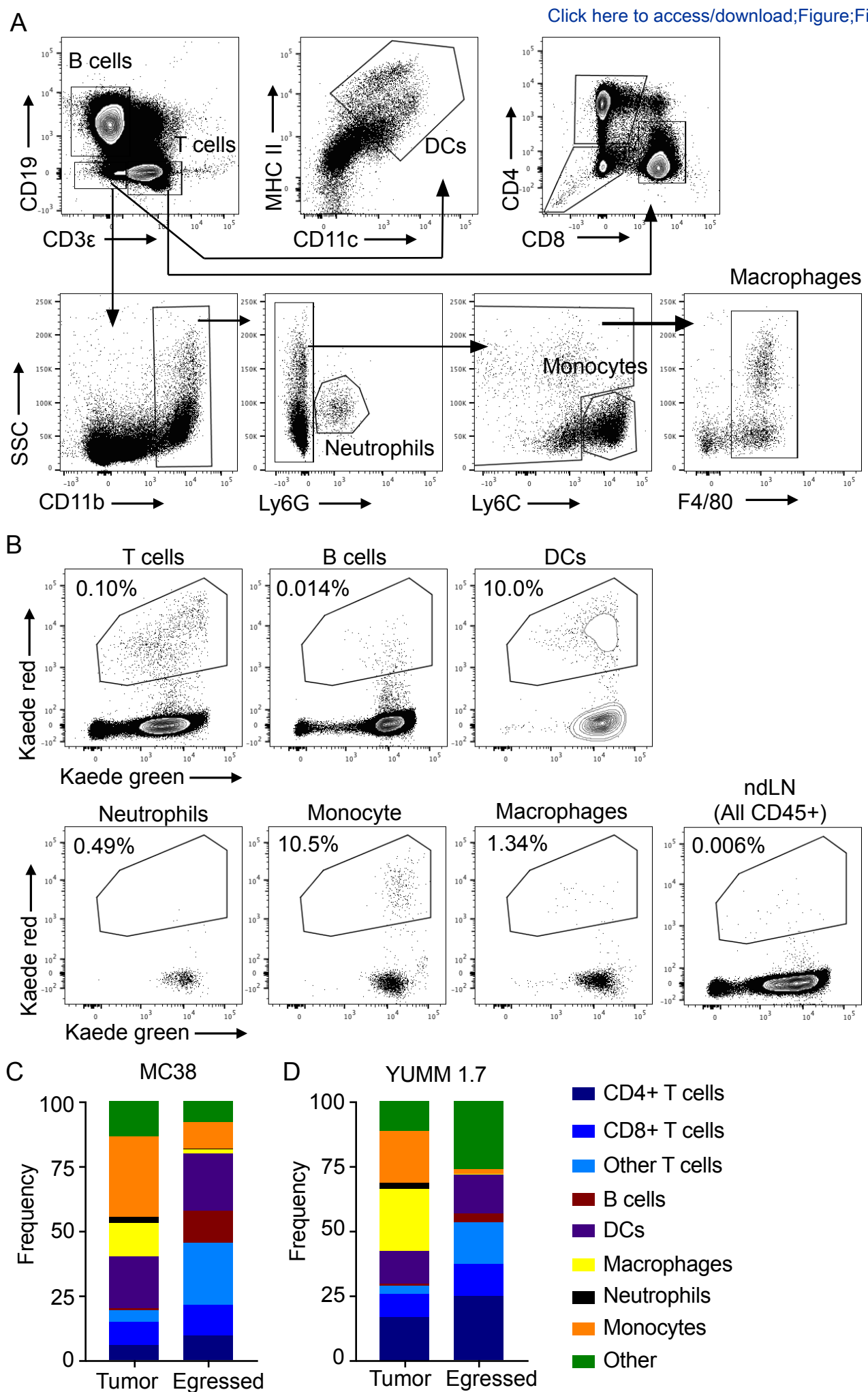


Figure 4

[Click here to access/download;Figure;Figure 4.pdf](#)



Name of Material/ Equipment	Company	Catalog Number
Collagenase D	Roche	11088866001
DNase	Roche	4536282001
Silver-LED-405B light source with optical fiber and collimator	Prizmatix Ltd	V8144
Fluorescein isothiocyanate isomer I	Sigma-Aldrich	F4274
dibutyl phthalate	Sigma-Aldrich	524980
acetone	Macron Fine Chemicals	2440-02
29-gauge syringes	Exel International	26029
Evans Blue	Sigma-Aldrich	E2129
70 um cell strainers	VWR	732-2758
paraformaldehyde	Sigma-Aldrich	P6148
HBSS	Caisson	HBL06
LIVE/DEAD Fixable Aqua Dead Cell Stain Kit	Invitrogen	L34966
Purified Anti-mouse CD16/CD32	Tonbo Biosciences	70-0161-M001
BV605 CD11c (clone N418)	Biolegend	117334
PerCP-Cy5.5 MHCII (clone M5/114.15.2)	BD Pharmingen	562363
BV421 CD3e (clone 145-2C11)	Biolegend	100341
APC CD8a (clone 53-6.7)	TonBo Biosciences	20-0081-u100
APC-Cy7 CD45 (clone 30-F11)	Biolegend	103116
BV650 CD19 (clone 6D5)	Biolegend	115541
PercCP-Cy5.5 Ly6C (clone HK1.4)	Biolegend	128011
Alexa Fluor 647 F4/80 (clone BM8)	Biolegend	123121
APC-Cy7 Ly6G (clone 1A8)	Biolegend	127623
BV711 CD11b (clone M1/70)	Biolegend	101241
BV605 CD45 (clone 30-F11)	Biolegend	103155
BV711 CD4 (clone RM4-5)	BD Biosciences	563726
Bovine serum albumin (Fraction V)	Fisher Scientific	BP1600-100
Particle Set	BD Biosciences	552845
Fortessa Flow Cytometer	BD Biosciences	

FlowJo v10 Software

FlowJo

Comments/Description



1 Alewife Center #200
Cambridge, MA 02140
tel. 617.945.9051
www.jove.com

ARTICLE AND VIDEO LICENSE AGREEMENT

Title of Article: QUANTIFYING LEUKOCYTE EGRESS VIA LYMPHATIC VESSELS FROM MURINE SKIN AND THYROID

Author(s): STEELE MM, CHURCHILL MS, BREAZEALE AP, LAWERS, NELSON NA, LUND AW

Item 1 (check one box): The Author elects to have the Materials be made available (as described at

http://www.jove.com/author) via: ☒ Standard Access ☐ Open Access

Item 2 (check one box):

- ☒ The Author is NOT a United States government employee.
- ☐ The Author is a United States government employee and the Materials were prepared in the course of his or her duties as a United States government employee.
- ☐ The Author is a United States government employee but the Materials were NOT prepared in the course of his or her duties as a United States government employee.

ARTICLE AND VIDEO LICENSE AGREEMENT

1. **Defined Terms.** As used in this Article and Video License Agreement, the following terms shall have the following meanings: "**Agreement**" means this Article and Video License Agreement; "**Article**" means the article specified on the last page of this Agreement, including any associated materials such as texts, figures, tables, artwork, abstracts, or summaries contained therein; "**Author**" means the author who is a signatory to this Agreement; "**Collective Work**" means a work, such as a periodical issue, anthology or encyclopedia, in which the Materials in their entirety in unmodified form, along with a number of other contributions, constituting separate and independent works in themselves, are assembled into a collective whole; "**CRC License**" means the Creative Commons Attribution-Non Commercial-No Derivs 3.0 Unported Agreement, the terms and conditions of which can be found at: <http://creativecommons.org/licenses/by-nc-nd/3.0/legalcode>; "**Derivative Work**" means a work based upon the Materials or upon the Materials and other pre-existing works, such as a translation, musical arrangement, dramatization, fictionalization, motion picture version, sound recording, art reproduction, abridgment, condensation, or any other form in which the Materials may be recast, transformed, or adapted; "**Institution**" means the institution, listed on the last page of this Agreement, by which the Author was employed at the time of the creation of the Materials; "**JoVE**" means MyJoVE Corporation, a Massachusetts corporation and the publisher of *The Journal of Visualized Experiments*; "**Materials**" means the Article and / or the Video; "**Parties**" means the Author and JoVE; "**Video**" means any video(s) made by the Author, alone or in conjunction with any other parties, or by JoVE or its affiliates or agents, individually or in collaboration with the Author or any other parties, incorporating all or any portion of the Article, and in which the Author may or may not appear.

2. **Background.** The Author, who is the author of the Article, in order to ensure the dissemination and protection of the Article, desires to have the JoVE publish the Article and create and transmit videos based on the Article. In furtherance of such goals, the Parties desire to memorialize in this Agreement the respective rights of each Party in and to the Article and the Video.

3. **Grant of Rights in Article.** In consideration of JoVE agreeing to publish the Article, the Author hereby grants to JoVE, subject to **Sections 4 and 7** below, the exclusive, royalty-free, perpetual (for the full term of copyright in the Article, including any extensions thereto) license (a) to publish, reproduce, distribute, display and store the Article in all forms, formats and media whether now known or hereafter developed (including without limitation in print, digital and electronic form) throughout the world, (b) to translate the Article into other languages, create adaptations, summaries or extracts of the Article or other Derivative Works (including, without limitation, the Video) or Collective Works based on all or any portion of the Article and exercise all of the rights set forth in (a) above in such translations, adaptations, summaries, extracts, Derivative Works or Collective Works and (c) to license others to do any or all of the above. The foregoing rights may be exercised in all media and formats, whether now known or hereafter devised, and include the right to make such modifications as are technically necessary to exercise the rights in other media and formats. If the "Open Access" box has been checked in **Item 1** above, JoVE and the Author hereby grant to the public all such rights in the Article as provided in, but subject to all limitations and requirements set forth in, the CRC License.

ARTICLE AND VIDEO LICENSE AGREEMENT

4. Retention of Rights in Article. Notwithstanding the exclusive license granted to JoVE in **Section 3** above, the Author shall, with respect to the Article, retain the non-exclusive right to use all or part of the Article for the non-commercial purpose of giving lectures, presentations or teaching classes, and to post a copy of the Article on the Institution's website or the Author's personal website, in each case provided that a link to the Article on the JoVE website is provided and notice of JoVE's copyright in the Article is included. All non-copyright intellectual property rights in and to the Article, such as patent rights, shall remain with the Author.

5. Grant of Rights in Video – Standard Access. This **Section 5** applies if the "Standard Access" box has been checked in **Item 1** above or if no box has been checked in **Item 1** above. In consideration of JoVE agreeing to produce, display or otherwise assist with the Video, the Author hereby acknowledges and agrees that, Subject to **Section 7** below, JoVE is and shall be the sole and exclusive owner of all rights of any nature, including, without limitation, all copyrights, in and to the Video. To the extent that, by law, the Author is deemed, now or at any time in the future, to have any rights of any nature in or to the Video, the Author hereby disclaims all such rights and transfers all such rights to JoVE.

6. Grant of Rights in Video – Open Access. This **Section 6** applies only if the "Open Access" box has been checked in **Item 1** above. In consideration of JoVE agreeing to produce, display or otherwise assist with the Video, the Author hereby grants to JoVE, subject to **Section 7** below, the exclusive, royalty-free, perpetual (for the full term of copyright in the Article, including any extensions thereto) license (a) to publish, reproduce, distribute, display and store the Video in all forms, formats and media whether now known or hereafter developed (including without limitation in print, digital and electronic form) throughout the world, (b) to translate the Video into other languages, create adaptations, summaries or extracts of the Video or other Derivative Works or Collective Works based on all or any portion of the Video and exercise all of the rights set forth in (a) above in such translations, adaptations, summaries, extracts, Derivative Works or Collective Works and (c) to license others to do any or all of the above. The foregoing rights may be exercised in all media and formats, whether now known or hereafter devised, and include the right to make such modifications as are technically necessary to exercise the rights in other media and formats. For any Video to which this Section 6 is applicable, JoVE and the Author hereby grant to the public all such rights in the Video as provided in, but subject to all limitations and requirements set forth in, the CRC License.

7. Government Employees. If the Author is a United States government employee and the Article was prepared in the course of his or her duties as a United States government employee, as indicated in **Item 2** above, and any of the licenses or grants granted by the Author hereunder exceed the scope of the 17 U.S.C. 403, then the rights granted hereunder shall be limited to the maximum rights permitted under such

statute. In such case, all provisions contained herein that are not in conflict with such statute shall remain in full force and effect, and all provisions contained herein that do so conflict shall be deemed to be amended so as to provide to JoVE the maximum rights permissible within such statute.

8. Likeness, Privacy, Personality. The Author hereby grants JoVE the right to use the Author's name, voice, likeness, picture, photograph, image, biography and performance in any way, commercial or otherwise, in connection with the Materials and the sale, promotion and distribution thereof. The Author hereby waives any and all rights he or she may have, relating to his or her appearance in the Video or otherwise relating to the Materials, under all applicable privacy, likeness, personality or similar laws.

9. Author Warranties. The Author represents and warrants that the Article is original, that it has not been published, that the copyright interest is owned by the Author (or, if more than one author is listed at the beginning of this Agreement, by such authors collectively) and has not been assigned, licensed, or otherwise transferred to any other party. The Author represents and warrants that the author(s) listed at the top of this Agreement are the only authors of the Materials. If more than one author is listed at the top of this Agreement and if any such author has not entered into a separate Article and Video License Agreement with JoVE relating to the Materials, the Author represents and warrants that the Author has been authorized by each of the other such authors to execute this Agreement on his or her behalf and to bind him or her with respect to the terms of this Agreement as if each of them had been a party hereto as an Author. The Author warrants that the use, reproduction, distribution, public or private performance or display, and/or modification of all or any portion of the Materials does not and will not violate, infringe and/or misappropriate the patent, trademark, intellectual property or other rights of any third party. The Author represents and warrants that it has and will continue to comply with all government, institutional and other regulations, including, without limitation all institutional, laboratory, hospital, ethical, human and animal treatment, privacy, and all other rules, regulations, laws, procedures or guidelines, applicable to the Materials, and that all research involving human and animal subjects has been approved by the Author's relevant institutional review board.

10. JoVE Discretion. If the Author requests the assistance of JoVE in producing the Video in the Author's facility, the Author shall ensure that the presence of JoVE employees, agents or independent contractors is in accordance with the relevant regulations of the Author's institution. If more than one author is listed at the beginning of this Agreement, JoVE may, in its sole discretion, elect not take any action with respect to the Article until such time as it has received complete, executed Article and Video License Agreements from each such author. JoVE reserves the right, in its absolute and sole discretion and without giving any reason therefore, to accept or decline any work submitted to JoVE. JoVE and its employees, agents and independent contractors shall have

ARTICLE AND VIDEO LICENSE AGREEMENT

full, unfettered access to the facilities of the Author or of the Author's institution as necessary to make the Video, whether actually published or not. JoVE has sole discretion as to the method of making and publishing the Materials, including, without limitation, to all decisions regarding editing, lighting, filming, timing of publication, if any, length, quality, content and the like.

11. **Indemnification.** The Author agrees to indemnify JoVE and/or its successors and assigns from and against any and all claims, costs, and expenses, including attorney's fees, arising out of any breach of any warranty or other representations contained herein. The Author further agrees to indemnify and hold harmless JoVE from and against any and all claims, costs, and expenses, including attorney's fees, resulting from the breach by the Author of any representation or warranty contained herein or from allegations or instances of violation of intellectual property rights, damage to the Author's or the Author's institution's facilities, fraud, libel, defamation, research, equipment, experiments, property damage, personal injury, violations of institutional, laboratory, hospital, ethical, human and animal treatment, privacy or other rules, regulations, laws, procedures or guidelines, liabilities and other losses or damages related in any way to the submission of work to JoVE, making of videos by JoVE, or publication in JoVE or elsewhere by JoVE. The Author shall be responsible for, and shall hold JoVE harmless from, damages caused by lack of sterilization, lack of cleanliness or by contamination due to the making of a video by JoVE its employees, agents or independent contractors. All sterilization, cleanliness or decontamination procedures shall be solely the responsibility of the Author and shall be undertaken at the Author's

expense. All indemnifications provided herein shall include JoVE's attorney's fees and costs related to said losses or damages. Such indemnification and holding harmless shall include such losses or damages incurred by, or in connection with, acts or omissions of JoVE, its employees, agents or independent contractors.

12. **Fees.** To cover the cost incurred for publication, JoVE must receive payment before production and publication the Materials. Payment is due in 21 days of invoice. Should the Materials not be published due to an editorial or production decision, these funds will be returned to the Author. Withdrawal by the Author of any submitted Materials after final peer review approval will result in a US\$1,200 fee to cover pre-production expenses incurred by JoVE. If payment is not received by the completion of filming, production and publication of the Materials will be suspended until payment is received.

13. **Transfer, Governing Law.** This Agreement may be assigned by JoVE and shall inure to the benefits of any of JoVE's successors and assignees. This Agreement shall be governed and construed by the internal laws of the Commonwealth of Massachusetts without giving effect to any conflict of law provision thereunder. This Agreement may be executed in counterparts, each of which shall be deemed an original, but all of which together shall be deemed to be one and the same agreement. A signed copy of this Agreement delivered by facsimile, e-mail or other means of electronic transmission shall be deemed to have the same legal effect as delivery of an original signed copy of this Agreement.

A signed copy of this document must be sent with all new submissions. Only one Agreement required per submission.

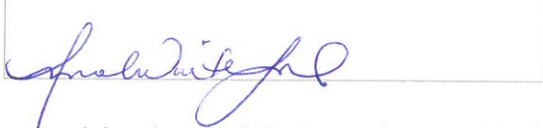
CORRESPONDING AUTHOR:

Name: AMANDA W. LUND

Department: CELL, DEVELOPMENTAL, & CANCER BIOLOGY

Institution: OREGON HEALTH & SCIENCE UNIVERSITY

Article Title: QUANTIFYING LEUKOCYTE EGRESS VIA LYMPHATIC VESICLES FROM MURINE SKIN AND TUMORS

Signature:  Date: 6/29/2018

Please submit a signed and dated copy of this license by one of the following three methods:

- 1) Upload a scanned copy of the document as a pdf on the JoVE submission site;
- 2) Fax the document to +1.866.381.2236;
- 3) Mail the document to JoVE / Attn: JoVE Editorial / 1 Alewife Center #200 / Cambridge, MA 02139

For questions, please email submissions@jove.com or call +1.617.945.9051

Editorial comments:

The manuscript has been modified and the updated manuscript, **58704_R1.docx**, is attached and located in your Editorial Manager account. **Please use the updated version to make your revisions.**

1. Please take this opportunity to thoroughly proofread the manuscript to ensure that there are no spelling or grammar issues.

The manuscript has been reviewed for spelling and grammar issues.

2. Please use standard SI unit symbols and prefixes such as μL , mL, L, g, m, etc.

SI units have been added.

3. Please use h, min, s for time units.

All time units have been adjusted.

4. Please do not highlight notes for filming.

Highlighting of notes have been removed.

5. Please do not highlight any steps describing euthanasia or anesthesia.

Highlighted steps including euthanasia have been removed.

6. Please remove all headers from Representative Results.

Headers have been removed.